RSC Advances

PAPER

View Article Online
View Journal | View Issue

Cite this: *RSC Adv.*, 2025, **15**, 23396

Composite materials containing Brønsted acid sites derived from *Syzygium nervosum* leaves *via* graphene oxide modification as green catalysts for the synthesis of 4-thiazolidinones†

Quang Nhat Trinh,[ab] Linh Dieu Nguyen [ab] and Hai Truong Nguyen *[ab]

An IL@SGO catalyst was synthesized from leaf residues of *Syzygium nervosum via* the modification of sulfur-doped graphene oxide (SGO) with dual-acid ionic liquid 3-(3-sulfopropyl)-1-(3-(triethoxysilyl) propyl)-1*H*-imidazol-3-ium hydrosulfate (IL) and used for the synthesis of a 4-thiazolidinone framework with diverse biological activities. The structure and morphology of IL@SGO were determined using modern physical techniques such as FT-IR spectroscopy, Raman spectroscopy, XRD analysis, ICP-MS analysis, scanning electron microscopy (SEM), energy-dispersive X-ray spectroscopy (EDX), and thermogravimetric analysis (TGA). It is anticipated that in the future, the IL@SGO catalyst will emerge as a promising catalyst with its unique and environmentally friendly characteristics. The reaction was carried out at 80 °C for 9 hours in the presence of toluene (5 mL) and IL@SGO (7 mg), and a major product was obtained in a yield ranging from 10% to 49%. Derived from *Syzygium nervosum* leaves, the IL@SGO catalyst exhibited enhanced acidity and proton conductivity, thereby improving the yield and enabling catalyst recovery and reuse that contribute to environmental preservation.

Received 25th April 2025
Accepted 25th June 2025

DOI: 10.1039/d5ra02881g

rsc.li/rsc-advances

1. Introduction

Currently, the consumption of graphite is increasing, and the environmental degradation caused by the graphite mining process has recently attracted attention, necessitating the development of sustainable chemistry. Carbon biomass was considered a unique renewable raw material on earth, seen as a potential substitute for natural graphite formed in metamorphic rock deposits or in areas with volcanic rock, which is a non-renewable fuel in the short term.[1] Special "green" materials include biomass-derived catalysts due to their low cost, reusability, recoverability, abundant supply, efficient production procedures, and environmental friendliness. Since 2016, numerous effective approaches for solid acid-base catalyst production using marine animal shells, animal bones, and plant waste have been disclosed.[2] Using plant leaves, particularly those from *Syzygium nervosum*, offers several definitive advantages over commercially available graphite powder. The carbonization of leaves to produce graphite powder is a sustainable alternative to non-renewable, environmentally harmful mining. Biomass materials such as agricultural waste are often cheaper due to their abundance, and their use promotes economic sustainability. The synthesis process involves both oxidation and functionalization steps, which introduce oxygen-containing functional groups. These groups enhance the catalyst's activity, particularly improving its performance in environments with high acidity and proton conductivity.

Graphene is a noteworthy carbon material with a 2D structure composed of sp^2 hybridized carbon atoms arranged in a hexagonal pattern, creating a large surface area on both sides of the flat plane. Graphene-derived materials, such as few-layer graphene, GO, and rGO, represent structurally and chemically modified forms with tailored functionalities.[3] GO are 2D materials like bulk graphene, with stable covalent bonds within the layers, which is synthesized through the oxidation of graphene. After oxidation, the material's surface forms oxygen-containing anionic groups such as epoxy (–C–O–C), hydroxyl (–OH), carboxyl (–COOH), and carbonyl (–C=O) groups. Additionally, GO has unique outstanding properties such as mechanical stability, high surface area, and good dispersion in various environments. Therefore, it frequently serves as a catalyst.[4–6] To synthesize GO from biomass, a carbonization process is commonly used, primarily utilizing agricultural and forestry waste rich in cellulose, hemicellulose, and lignin. These materials, due to their high carbon content, can be converted into porous carbon through carbonization at high pyrolysis temperatures and under oxygen-limited conditions. Studies

[a]*Department of Organic Chemistry, Faculty of Chemistry, University of Science, Ho Chi Minh City, 700000, Vietnam. E-mail: ngthai@hcmus.edu.vn; Tel: +84-908-108-824*
[b]*Vietnam National University, Ho Chi Minh City, 700000, Vietnam*

† Electronic supplementary information (ESI) available. See DOI: https://doi.org/10.1039/d5ra02881g

have successfully used sources such as wood, tea leaves, sugarcane bagasse, fruit peels, and chicken bones to modify graphite into GO using Hummer's synthesis method.[7] The advantages of GO materials are high surface area, electrical conductivity, mechanical strength, and the ability to be easily functionalized, which are key factors that make GO an attractive platform for the development of advanced materials.[8] Traditional liquid acid catalysts show some disadvantages such as corrosion, environmental impact, and difficulty in separation from the reaction mixture.[9] The materials containing Brønsted acid sites derived *via* GO modification signify a notable advancement in materials science, merging the outstanding characteristics of GO with the catalytic benefits of Brønsted acids.[10] The modification of GO with Brønsted acid sites can be made through various methods such as direct functionalization of GO with acidic compounds, grafting of acid-functionalized polymers, or impregnation with acidic salts.[11] The high surface area of GO facilitates effective charge storage in supercapacitors and batteries, and the acidic sites help in the elimination of contaminants from wastewater *via* adsorption or catalytic degradation. Moreover, the combination of Brønsted acid sites with GO improves the mechanical characteristics of the material, facilitating the creation of stronger and more resilient composites and coatings.[12,13]

The synthesis of 4-thiazolidinone plays a vital role in the field of pharmaceutical due to its potential biological activity and its presence in various bioactive nature compounds.[14] 4-Thiazolidinone is a five-membered heterocyclic compound containing both sulfur (S) and nitrogen (N) atoms in its structure, making it highly significant due to its pharmacological properties.[14] The 4-thiazolidinone derivatives exhibit many important biological activities including antimicrobial,[15] antitumor,[16,17] anticonvulsant,[18] anti-inflammatory,[19] and antioxidant[20] effects. Based on the versatility and bioactivity of this compound, the development of efficient and novel synthetic pathways becomes a key focus in synthetic chemistry. Several synthetic approaches have been proposed to construct the 4-thiazolidinone frame, each method using different starting materials and reaction conditions. Some of the most common methods are cyclization reactions with thiol derivatives or thioureas, and isothiocyanates or α,β-unsaturated carbonyl compounds.[21] One of the most widely used methods to synthesize 4-thiazolidinone is the cyclization reaction of thiourea derivatives and α,β-unsaturated carbonyl compounds.[21] The reaction commonly proceeds *via* a nucleophilic attack, leading to the formation of a five-membered thiazolidine ring with good yields and selectivity for 4-thiazolidinone, and is applied to a wide range of substrates, allowing for the functionalization of the desired products. Another synthetic pathway involves the reaction of isothiocyanates with amines or thiols, leading to the formation of a thiazolidine ring with the sulfur atom incorporated into the structure.[22] Researchers had also explored multi-component reactions for the synthesis of 4-thiazolidinones, which provided the advantage of a one-pot synthesis.[23] A typical multi-component reaction (MCR) may include the condensation of thiols, amines, and α,β-unsaturated carbonyl compounds to directly produce 4-thiazolidinones without isolating intermediate compounds. This approach enhances the yield, reduces the number of steps, and decreases waste, making it a highly appealing option for large-scale synthesis.[24] 4-Thiazolidinone can be modified to produce several derivatives with improved or customized biological characteristics. The ability to modify the structure at different positions of the thiazolidinone ring, particularly at the 2- or 5-positions, provides opportunities for developing compounds with specific interactions with biological targets.[25] Integrating green chemistry concepts such as solvent-free reactions, catalytic techniques, and sustainable reagents can enhance the efficiency and ecological sustainability of 4-thiazolidinone synthesis. In conclusion, synthesizing 4-thiazolidinone is vital for drug development, offering various synthetic routes to create diverse derivatives with significant biological activities. Ongoing advancements in synthetic techniques and continued research on these derivatives in preclinical and clinical settings suggest they will play an important role in developing new therapies for various disorders.

The aim of the research is to outline the novel synthesis route of 3-(3-sulfopropyl)-1-(3-(triethoxysilyl)propyl)-1*H*-imidazol-3-ium hydrosulfate (IL) with sulfur-doped graphene oxide (SGO) derived from *Syzygium nervosum* leaves to generate 4-thiazolidinone derivatives. The reaction involving benzaldehydes (1 mmol), anilines (1 mmol), and mercaptoacetic acid (1 mmol) was selected as a model to synthesize 4-thiazolidinone derivatives, owing to its significance in evaluating the catalytic efficiency of IL@SGO. IL@SGO, a composite material containing Brønsted acid sites derived *via* graphene oxide modification, had a highly reactive surface for the reaction, facilitating an efficient and environmentally benign method for thiazolidinone production. This reaction acts as a realistic standard to illustrate the material's catalytic efficacy under mild conditions. This catalyst is reusable and promotes eco-friendly practices *via* a one-pot, multi-component reaction process.

2. Results and discussion

2.1. Characterization of ionic liquid-functionalized sulfur-doped graphite oxide (IL@SGO)

Scheme 1 illustrates the process of anchoring 3-(3-sulfopropyl)-1-(3-(triethoxysilyl)propyl)-1*H*-imidazol-3-ium hydrosulfate (IL) onto sulfur-doped graphene oxide to synthesize the material IL@SGO. Initially, *Syzygium nervosum* leaves were carbonized at 650 °C for 3 hours to prepare the graphite powder.[26] Using Hummer's method with $KMnO_4$, $NaNO_3$, and H_2SO_4, the graphite was oxidized to GO, introducing oxygen-containing functional groups.[27] GO was modified with aryl diazonium compounds to add sulfonic acid ($-SO_3H$) groups to form SGO.[28] IL was synthesized *via* a three-step process: imidazole reacts with CPTES at 110 °C for 12 hours, then, 1,4-butanesultone was added into the mixture at room temperature for 8 hours, and finally, H_2SO_4 was added to the mixture in the presence of ethanol at 50 °C for 8 hours.[29] The IL was integrated with SGO, resulting in the hybrid material IL@SGO.[29] The structure and surface chemistry of IL@SGO materials were determined by Fourier transform infrared (FT-IR) spectroscopy, Raman

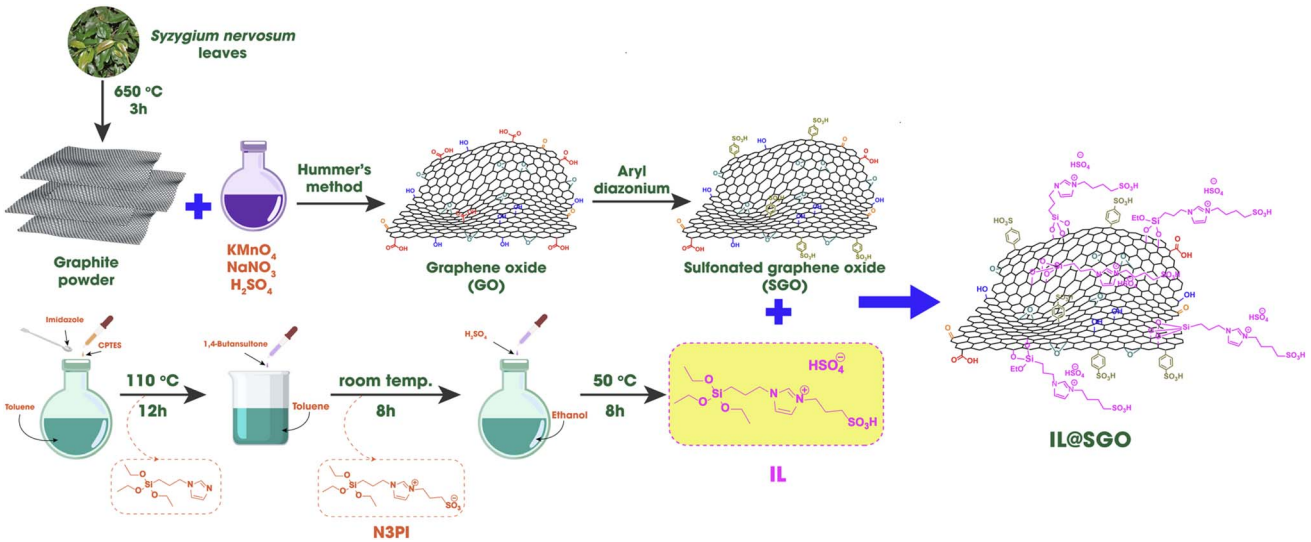

Scheme 1 Preparation process of the IL@SGO material from *Syzygium nervosum* leaves.

spectroscopy, X-ray diffraction (XRD), inductively coupled plasma-mass spectrometry (ICP-MS), scanning electron microscopy (SEM), energy-dispersive X-ray spectroscopy (EDX), and thermogravimetric analysis (TGA).

The FT-IR spectra presented the comparison between several materials, which were prepared from each stage, including graphite, graphene oxide (GO), sulfur-doped graphene oxide (SGO), a double acidic IL, and IL-functionalized sulfur-doped graphene oxide (IL@SGO) (Fig. 1). The broad absorption band around 3500–3300 cm^{-1} was most prominent in the spectra of graphite and GO, which indicated the presence of hydroxyl groups of the phenol and alcohol. In GO materials, these hydroxyl groups resulted from the oxidative treatment of graphite, which introduced oxygen-containing functionalities to the basal planes and edges of the GO sheets. The –OH band weakened in the SGO material because some hydroxyl groups were partially removed or chemically transformed during the sulfur doping process. In the IL@SGO material, the –OH band diminished further, suggesting that the IL functionalization either consumed these groups or masked their vibrational signal due to the introduction of new bulky organic groups. The peak at 1720 cm^{-1} was assigned to the stretching vibrations of carbonyl groups (C=O) in carboxylic acids or esters, formed during the oxidative process of the GO material alongside hydroxyl and epoxy groups. In the SGO material, the C=O peak slightly shifted and reduced in intensity, indicating that sulfur doping partially decreased carboxyl groups or changed them into sulfonic acid or thiol groups. The peaks observed in the range of 1200–1250 cm^{-1} corresponded to C–O–C vibrations from epoxy and ether groups, which were prominent in GO due to the oxidative introduction of these oxygen-containing functionalities. In IL@SGO material, these peaks were almost absent, reflecting further chemical modifications during IL functionalization. The reduction or modification of these groups enhanced hydrophobicity and reduced oxygenated surface chemistry. Absorption bands between 3000 and 2800 cm^{-1} were characteristic of stretching vibrations from aliphatic C–H bonds. These bands were most intense in IL and IL@SGO, indicating the introduction of organic groups from the IL. The peaks in the range of 1000–1100 cm^{-1} were attributed to sulfur-oxygen bonds such as sulfoxides (S=O) or sulfates. These peaks were a clear indication of sulfur doping in SGO, where sulfur atoms are incorporated into the structure through chemical modifications. In the IL@SGO material, the intensity of these peaks increased, which showed that the IL functionalization stabilized the sulfur-containing groups or enhanced their vibrational signals. Peaks around 1600–1650 cm^{-1} were observed in the spectra of IL and IL@SGO, which were associated with the stretching vibrations of C=C and C=N bonds within the imidazole ring of the IL. A comparative analysis between GO and SGO revealed that sulfur doping reduced oxygen-containing groups such as hydroxyls, carbonyls, and epoxies. The decrease was evidenced by the

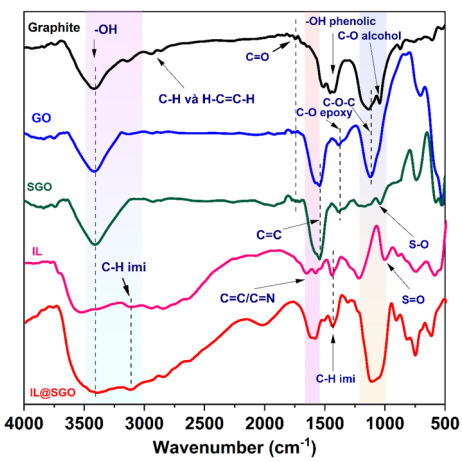

Fig. 1 FT-IR spectra of four components (graphite, GO, SGO, and IL) and IL@SGO.

decreased intensity of the –OH, C=O and C–O–C signals in the SGO material. The incorporation of sulfur likely replaced these groups with sulfur-containing functionalities, which improved the chemical reactivity.[30] The FT-IR spectra demonstrated a systematic evolution of chemical functionalities from GO to SGO and finally to IL@SGO.[31] The successful incorporation of sulfur and ILs suggests that IL@SGO is a multifunctional material with potential uses in catalysis, energy storage, and environmental remediation.[32–34]

Fig. 2 presents the X-ray Diffraction (XRD) patterns of five different materials, including graphite, GO (graphene oxide), SGO (sulfonated graphene oxide), IL (ionic liquid), and IL@SGO (IL encapsulated on sulfonated GO). The XRD pattern of graphite displayed many sharp and intense peaks, especially peaks at 2θ around 26.5°, 43.5° and 54.5° that correlate with the (002), (101), and (004) planes, respectively. The (002) peak position was the result of interlayer stacking carbon sheets of graphene over a hexagonal lattice along the *c*-axis, which was indicative of a high degree of crystalline and regular stacking of carbon layers. The resolution and pronounced characteristics of peaks confirmed that graphite was highly ordered, with high crystallinity and a low defect structure. This demonstrated that the GO presented substantial structural alterations from pristine graphite, with a sharp peak corresponding to the (001) plane at approximately $2\theta \approx 10$–12°. The lower angles compared to the (002) peak of graphite suggest an expansion of interlayer. A weak shoulder around $2\theta \approx 43°$ might indicate the residual graphitic domains or partial graphitization. Compared to GO, the (001) peak observed in SGO was broader and less intense, revealing loss of structural order resulting from sulfonation. The additional inclusion of sulfonic acid ($-SO_3H$) groups introduced defects and more disorder by breaking the regular stacking up even further. The wider peaks indicated decreasing crystallinity to give a more graphene-like arrangement in the material. The sulfonation procedure made SGO more hydrophilic and chemically reactive, therefore making it more applicable for catalytic and ion-exchange applications. In comparison to the other materials, the XRD pattern of IL was unique, with no sharp peaks and many broad background signals. This means that IL was not a crystalline material, therefore having no long-range periodic order. The general features seen here were typical for disordered molecular materials with ions located randomly throughout the structure. This fluidic phase was a characteristic feature of ILs due to the use of bulky, asymmetric cations and anions that impede the formation of a well-ordered regular lattice. The absence of crystalline features indicated that the material is mainly governed by weak van der Waals forces and ionic interactions that affect its thermal and physical properties. The IL@SGO composite material inherited the structural features of both SGO and IL, the pattern showing the broad features corresponding to the amorphous character of IL coupled with the low-intensity reflections corresponding to the partially crystalline nature of SGO. The presence of weak or fully suppressed peaks associated with the (001) and (002) planes confirmed strong interactions between the IL molecules and the SGO matrix. The disruption of stacking of GO layers could be further achieved with the encapsulation of IL within SGO, resulting in a more disordered structure of the hybrid material. A few weak diffraction peaks corresponded to the standard reference (JCPDS 00-041-1487), confirming that there are small crystalline phases, which may be due to impurities or partial crystallization in the synthesis process.

This image represented a Thermogravimetric Analysis (TGA) plot, which demonstrated the thermal stability and weight loss behavior of different materials as a function of temperature (Fig. 3). The current data referred to the thermal decomposition and stability of five materials, namely graphite, GO, SGO, IL, and IL@SGO. As can be seen, the graphite line had the most stable sample and shows almost no noticeable weight reduction during the heating period. Rather, it holds status for temperatures not exceeding 800 °C and even beyond. This implies that graphite can be used in extreme thermal applications and begins degenerating at above 800 °C, hence holding a minor weight loss, which can be assigned to the elimination of surface impurities or volatiles. The first weight loss in the TGA curves of GO observed at around 100 °C had been demonstrated as the

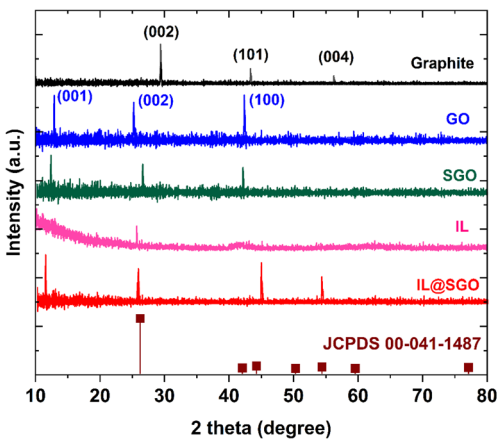

Fig. 2 XRD pattern of four components (graphite, GO, SGO, and IL) and IL@SGO.

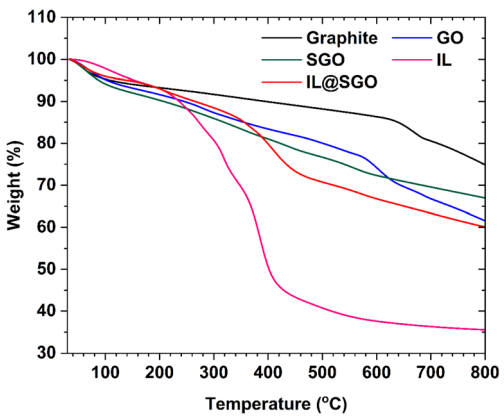

Fig. 3 TGA curve of four components (graphite, GO, SGO, and IL) and IL@SGO.

absorption of water.[35] GO began to show noticeable weight loss starting around 200–300 °C. This behavior was typically associated with the thermal decomposition of oxygen-containing functional groups, such as hydroxyl (–OH), carboxyl (–COOH), and epoxide (–C–O–C–) groups, which were present on the surface and edges of GO sheets.[36] The loss of weight continued until about 400 °C, when approximately 60% of the weight remains at 800 °C, which implied the existence of thermally labile groups in GO, these remaining stable at elevated temperatures, except for the carbon backbone. The shape of the SGO curve followed that of GO very closely, but with slight improvement in thermal stability, which is attributed to sulfuric acid. The structural sulfonic acid groups introduced by sulfonation enhance the chemical bonds and improved the stability from the thermal degradation. The thermal decomposition of SGO also started at around 200 °C but was much slower than that of GO, while it has the highest residual weight compared to the others at 800 °C. IL showed the most violent and rapid weight loss compared to other samples. The decomposition began at a very low temperature (about 200 °C) and total weight loss is observed by 500 °C, unlike most of the ILs, which decomposed at moderate temperatures because of the rupturing of the ionic framework or any other organic component. The sharp weight drop indicated that the IL is primarily composed of volatile components that were prone to evaporation or degradation under heat. The hybrid material IL@SGO demonstrates a three-step thermal decomposition process: The first stage (~100–200 °C) described the evaporation of water molecules, and the second stage (~200–400 °C) corresponded to the decomposition of IL components, like the behavior observed in the IL sample. Stage three (~400–700 °C) was ascribed to the heat degradation of the SGO backbone. The thermal stability of IL was also improved after incorporation into the SGO matrix in IL@SGO, as the weight loss was less notable than the IL alone. This phenomenon can be interpreted due to the interaction of the IL with the functional groups on SGO that limit the mobility and volatility of the IL molecules. Besides, based on the TGA results, the amount of ionic liquid attached can be predicted to be approximately 20%.

The SEM images and particle size distribution graphs offer a comparative interpretation of the structure of GO, SGO, and IL@SGO, which clearly represented the structural and morphological evolutions occurring during sulfur doping and ionic liquid modification (Fig. 4). As shown in Fig. 4, GO exhibited excellent dispersion and a large surface area due to its smooth, porous, and layered structures with low aggregation, in contrast to the rougher, wrinkled morphology of SGO. The addition of functional groups increased chemical reactivity and catalytic surface area. IL@SGO showed significant aggregation with many spherical particles forming on its surface, leading to a denser structure that may alter its conductivity and mechanical properties. Particle size analysis revealed that GO has the smallest size distribution (20–60 μm), indicating better dispersion, while SGO had a wider distribution with larger particles due to sulfur doping. IL@SGO had the broadest size range (20–100 μm) primarily due to ionic liquid-induced aggregation. Thus, while GO offered excellent dispersity for applications in adsorption, membrane technology, and sensors, the rougher texture of SGO made it suitable for catalytic reactions and energy storage. In contrast, the bulkier morphology of IL@SGO may enhance the supercapacitor performance, lubricants, or composite materials that required improved mechanical properties. This transition from GO to SGO to IL@SGO signified a trade-off between dispersion and aggregation, affecting their functional applications.

The image provided in Fig. 5 presents the EDX (Energy-Dispersive X-ray) spectra and corresponding elemental compositions of four samples: graphite, GO, SGO, and IL@SGO. The spectra and compositional data highlighted the structural and chemical changes during the transformation of graphite into GO, SGO, and IL@SGO. The EDX spectrum of graphite showed a dominant carbon peak (85.91% by mass, 89.39% by atom), indicating purity, with minimal oxygen (13.05% by mass) and trace elements of Si, S, and Cl probably due to environmental contamination. Upon converting graphite to GO, the carbon content decreased significantly to 65.47% by mass (72.53% by atom), while the oxygen content increased to 31.04% by mass (26.12% by atom), indicating the formation of functional groups from oxidation. Small peaks for sulfur (2.75%) and chlorine (0.2%) were attributed to Hummers' method or oxidation processes. The increase in oxygen disrupted the sp^2 hybridized structure, creating hydrophilic GO sheets. In IL@SGO, the carbon content further decreased to 26.04% by mass (32.38% by atom), with the oxygen content increasing to 68.87% by mass (64.29% by atom), suggesting enhanced functionalization. Sulfur peaks (1.51% by mass and 0.7% by atom) confirmed successful doping, while nitrogen (1.69% by mass and 1.8% by atom) indicated the presence of nitrogen-containing groups. IL@SGO showed carbon at 62.66% by mass (71.44% by atom) and oxygen at 25.1% by mass (21.49% by atom), with a higher sulfur fraction (4.33% by mass, 1.85% by atom) from the ionic liquid, along with increased chlorine (2.33%) and nitrogen (3.26%) contents due to functional groups from the IL. Overall, the transition from graphite to GO marked a shift from a carbon-rich structure to a highly oxidized material, initiating the functionalization process. Doping exemplified by the introduction of sulfur into SGO affords excellent doping, altering specific electronic and chemical properties of GO. The final modification with IL (IL@SGO) integrated additional functional groups, increasing sulfur and nitrogen contents while reducing excessive oxygen groups, resulting in a more balanced and functional material.[37–39]

The EDX mapping results revealed the elemental distribution and compositions of the samples (Fig. 6). Graphite and GO were found to have a high homogeneous intensity in the mapping of C (C-K), highlighting the fact that these materials contain more carbon than any other element. However, SGO and IL@SGO caused a tiny decrease in the carbon intensity due to the entrapment of new functional groups. The existence of Oxygen (O-K) was evident in GO, indicating the oxide formation of graphite; however, its intensity was diminished in SGO and IL@SGO, which might indicate the partial replacement or reaction of oxygen with functional groups. The content of K (potassium) was low in graphite and GO, and the amount of K

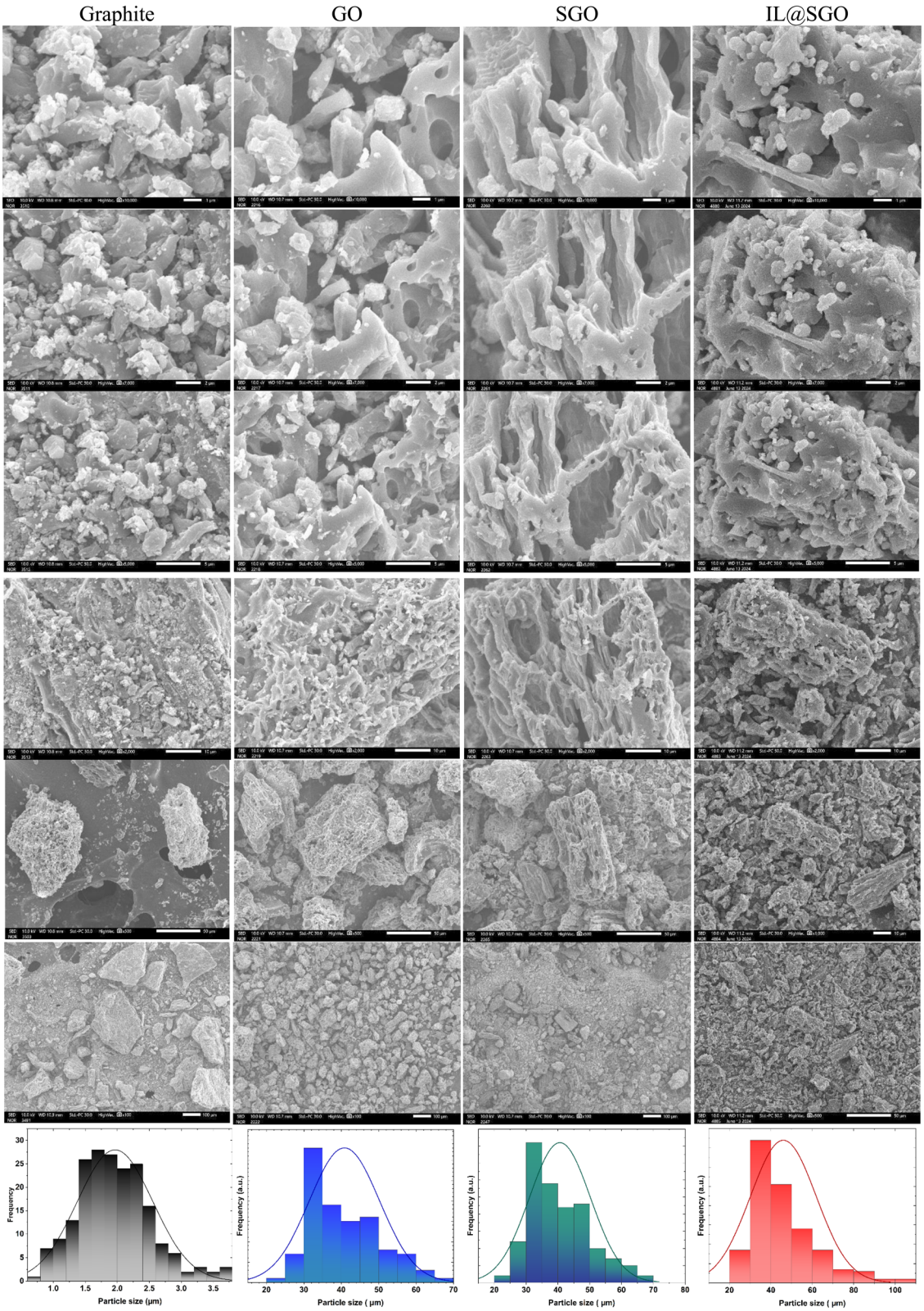

Fig. 4 SEM images and particle size distributions of three components (graphite, GO, and SGO) and IL@SGO.

increased markedly in SGO and IL@SGO (ion-liquid-modified reduced graphene oxide), confirming successful N-containing functionalization. Silicon (Si-K) popped only in SGO and IL@SGO, indicating silane-based modification(s) being implemented. IL@SGO showed a higher amount of sulfur (S-K) and chlorine (Cl-K), which may be attributed to the presence of

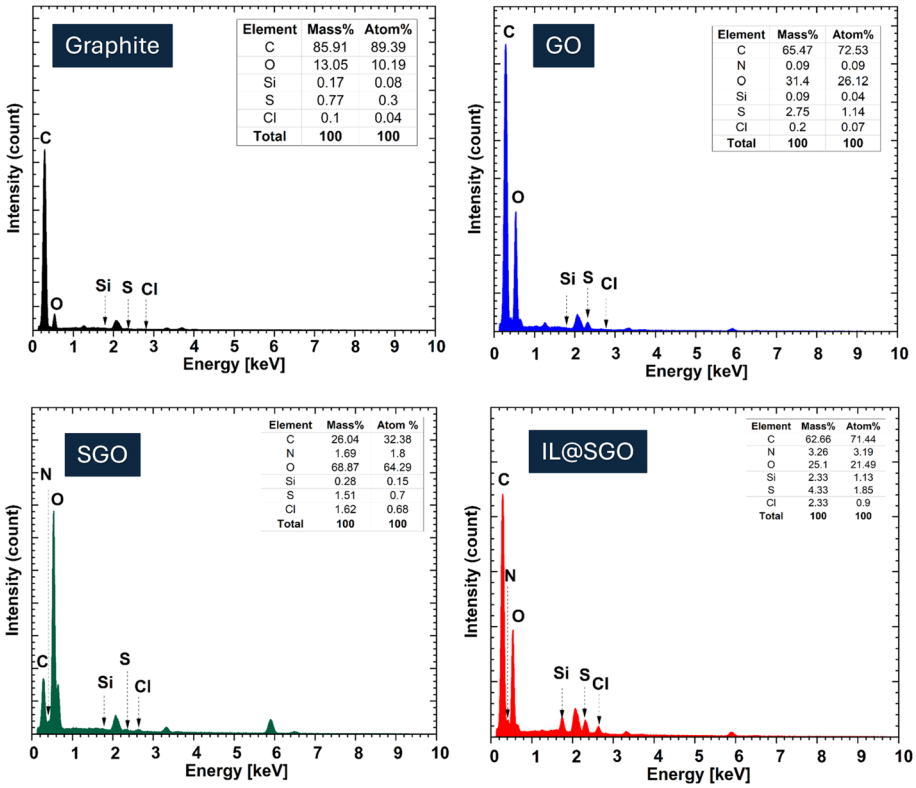

Fig. 5 Energy-dispersive X-ray (EDX) spectroscopy of three components (graphite, GO, and SGO) and IL@SGO.

sulfur-derived ILs or chlorinated species during the functionalization process. Specifically, graphite was mainly carbon, whereas GO added oxygen, SGO added nitrogen and silicon, and IL@SGO is the most functionally rich material, containing nitrogen, silicon, sulfur, and chlorine. Such results indicated the increasing chemical modification in the studied samples, and the most abundant elemental composition belongs to IL@SGO.

The Raman spectrum offered a comprehensive insight into the sample's chemical structure and composition (Fig. 7). The presence of peaks within this wavenumber range suggested the existence of silicon–oxygen–carbon (Si–O–C) bonds. These bonds were indicative of organosilicon compounds or silicon-containing framework materials. For example, a significant peak at about 511 cm^{-1} was related to vibrations of silicon observed in some silicon carbide (SiC) coatings. The D band (~1350 cm^{-1}), corresponding to the breathing modes of sp^2 carbon atoms in rings, was activated by defects or disorder in the carbon lattice. To quantify the degree of disorder, the intensity of the D band (I_D) was compared to that of the G band (I_G), resulting in the I_D/I_G ratio. This ratio served as a metric for assessing the level of structural imperfections. This means that a higher I_D/I_G ratio was suggestive of a higher amount of disorder or defects in the carbon framework. The band G (1600 cm^{-1}) was associated with the in-plane stretching modes of sp^2-hybridized carbon atoms. An obvious G band indicated graphitic or ordered carbon domains. The D and G band intensity ratio (I_D/I_G) typically correlated with the crystallinity and defect density of the carbon material. Based on previous research, the ratio intensity between D and G of graphene oxide was approximately 0.85.[40] In this study, as shown in the Raman spectra, the I_D/I_G value was calculated to be about 0.85, which illustrated the more amorphous carbon. This can be explained by the existence of sulfur in the structure of catalyst through the synthesis process. Besides, to confirm the appearance of sulfur in the structure of catalyst IL@SGO, the amount of sulfur in the product of each step was determined by ICP-OES. Consequently, the amount of sulfur in graphene oxide preparation step was calculated at about 35 376 mg g^{-1}, while the values of sulfur at the sulfonated stage and ionic liquid at the grafted stage were about 307 449 mg g^{-1} and 424 832 mg g^{-1}, respectively. The Raman spectrum and ICP-OES results of sulfur are strong evidence to prove the successful synthesis of the catalyst IL@SGO. The widespread peak in this area was characteristic of hydroxyl (–OH) groups (3000–3500 cm^{-1}), which corresponded to hydroxyl functionalities sorbed on the surface of material or water molecules adsorbed onto it. These groups may affect the hydrophilicity and reactivity of the material. The lower ratio implied a more oriented graphitic structure, while a higher ratio indicates more defects or more amorphous carbon.

BET surface characterization is an important aspect to analyze the surface area and porosity of the synthesized material. The characteristics of a matter are very much affected by the surface area-to-volume ratio. The GO, SGO, and IL@SGO catalytic pores and specific surface area were assessed (Fig. 8). The plots of GO showed a type II adsorption isotherm, which

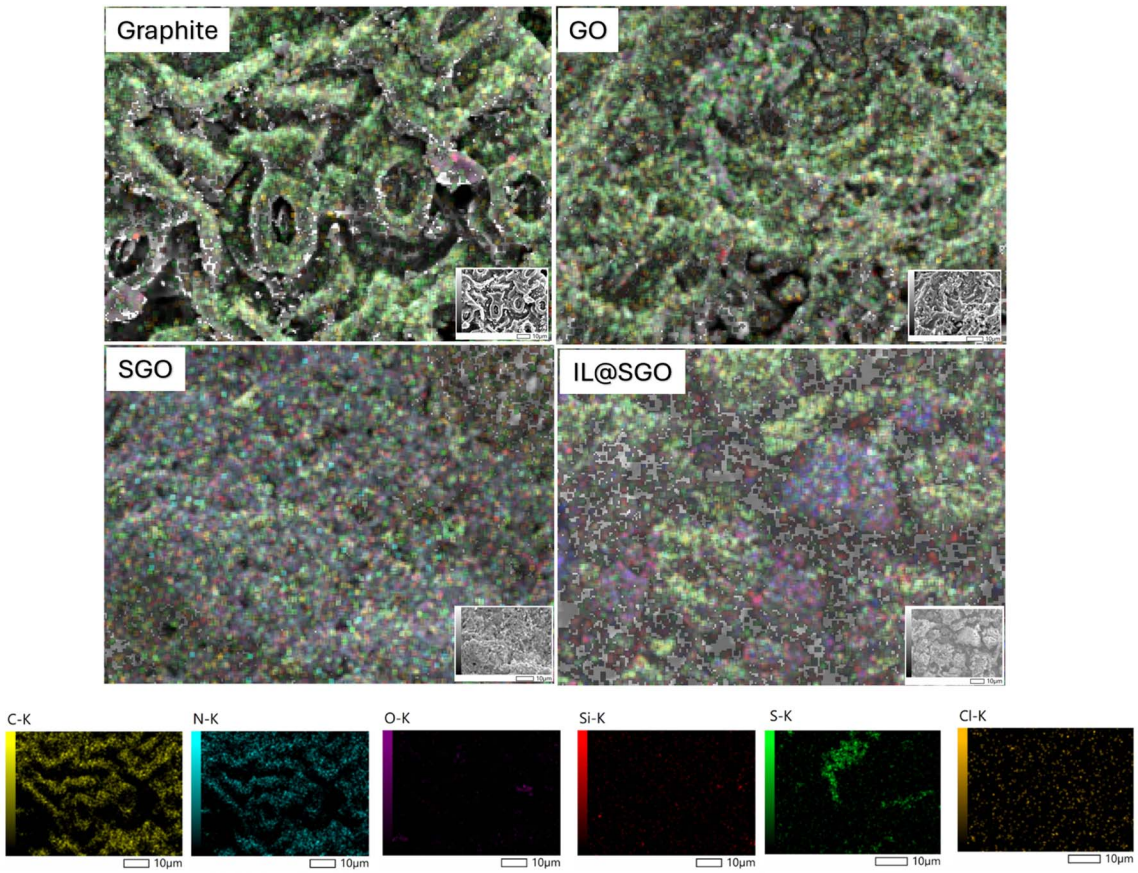

Fig. 6 EDX mapping of three components (graphite, GO, and SGO) and IL@SGO.

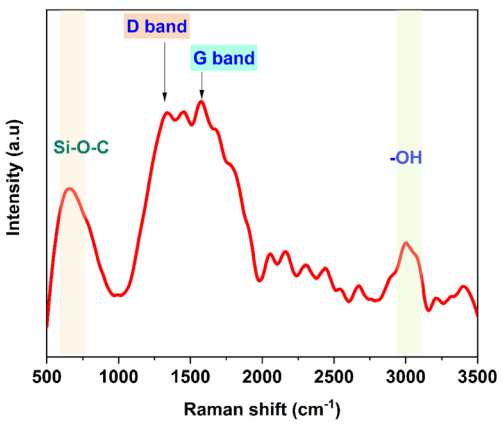

Fig. 7 Raman spectra of IL@SGO.

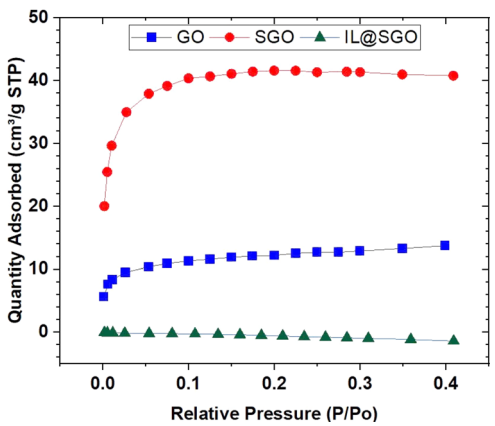

Fig. 8 Isotherm linear plots of GO, SGO, and IL@SGO catalysts.

was identified for non-porous or macroporous adsorbents exhibiting unrestricted monolayer-multilayer adsorption. The adsorption volume initially increased rapidly at low relative pressures when the adsorbate molecules engaged with the higher energy regions, subsequently interacting with the lower energy areas. After treating GO with acid, the plots of SGO demonstrated type I adsorption isotherm, which were applicable to adsorbents with extremely small pores or micropores. In this scenario, adsorption occurs through the filling of these micropores. IL@SGO illustrated that the quantity absorbed value remains at 0 for different relative pressures. It can be explained by the fact that grafting an ionic liquid reduces the porosity of the material. The catalyst surface area was measured to be 44.1 $m^2 g^{-1}$ for the GO catalyst and 135.1 $m^2 g^{-1}$ for the SGO catalyst, respectively. This suggested that the specific surface area of SGO and GO was much larger than that of IL@SGO, confirming the results of SEM characterization. The specific surface area of GO, SGO and IL@SGO was lower than

the range for the theoretically monolayer graphene oxide reported in the literature that is from 2 to 1000 $m^2 g^{-1}$, probably due to the agglomeration of the graphene sheets, giving partial overlap and coalescence, especially between the smaller sheets, thus reducing the surface area of the material.[41]

2.2. Catalytic activity of IL@SGO in the synthesis of 4-thiazolidinones

The one-pot multi-component reaction (MCR) technique is considered an ideal choice over traditional stepwise reactions involving several reactants. This is because stepwise methods are often time-intensive and result in significant product loss at each stage. In this study, we employed a pragmatic and very effective MCR methodology to synthesize the desired molecules. Benzaldehyde (1 mmol), aniline (1 mmol), and mercaptoacetic acid (1 mmol) were used as typical reactants to synthesize 2,3-diphenyl-4-thiazolidinone (**4aa**) (Scheme 2).

An experimental study of the isolated yield of a reaction under different temperatures, reaction times, solvent types, solvent volumes, catalyst types, and catalyst loadings is summarized in Table 1. Temperature is one of the key parameters that governs reaction kinetics and thermodynamics. At room temperature (r.t.), the reaction yield was only 16% (Table 1, Entry 1). As the temperature increased to 80 °C, yield increased up to 32% (Table 1, Entry 3). Higher temperatures may accelerate reaction rates by providing enough energy to overcome activation barriers. Increasing the temperature to 100 °C reduced the yield to 30% and to 29% at 120 °C (Entries 4–5, Table 1). The decline may be due to thermal degradation, evaporation of volatiles, or side reactions. The data indicated that the highest yield occurred at 80 °C. At 80 °C, shorter reaction times of 5 and 6 hours yielded 27% and 28%, respectively (Entries 6 and 7, Table 1), suggesting that the reaction had not yet reached completion. By extending the time to 9 hours, the yield reached a maximum of 37% (Entry 9, Table 1). It is worth mentioning, however, that increasing the reaction time to 10 hours did not improve the conversion (36%, Entry 10, Table 1). These results indicated equilibration after 9 hours, and that extending the reaction time was unlikely to give improved yields. Minimizing the resource consumption while maximizing the yield is critical to scale-up, achieved *via* the optimization reaction, *i.e.* reaction time for efficient reaction. The solvent selection influences the surrounding reaction environment such as solubility, polarity, and stabilization of intermediates, and therefore, it is the key to the reaction outcome. The best solvent, toluene, yielded 37% (Entry 9, Table 1). This may be attributed to its moderate polarity and compatibility with the reaction mechanism. In contrast, polar solvents such as ethanol (3%, Entry 11, Table 1), THF (13%, Entry 12, Table 1), and water (1%, Entry 13, Table 1) yielded lower results due to probable repulsive interactions with the catalyst or reactants. Similarly, nonpolar solvents such as cyclohexane (2%, Entry 17, Table 1) and *n*-hexane (5%, Entry 18, Table 1) performed poorly compared to extreme polar solvents. Chemical transformations often need to be optimized to balance solubility, reaction kinetics, and selectivity; therefore, solvent optimization is an important part of such optimization. Catalyst loading is a crucial parameter as it directly affects the availability of active sites, thus governing the efficiency of the reaction. Using IL@SGO as the catalyst, the yield increased from 30% with 1 mg (Entry 29, Table 1) to 42% with 7 mg (Entry 32, Table 1). Beyond this point, further increasing the catalyst loading to 10 mg resulted in a slight decline to 41% (Entry 33, Table 1). The observed trend suggested that too much catalyst may result in aggregation and lead to a lower catalysis surface area or diffusion limitations. The optimum catalyst loading was also highly dependent on the concentration of the catalytic component, as the overuse of resources would not only affect the cost-effectiveness of the process but also make it unfeasible to achieve a high throughput, posing a high barrier to commercialization. Catalyst performance was evaluated at 80 °C for 9 h. The hybrid catalyst IL@SGO gave the highest yield of 37% (Entry 9, Table 1) compared to GO (25%, Entry 20, Table 1), SGO (32%, Entry 21, Table 1), and IL (31%, Entry 22, Table 1). While H_2SO_4 (Entry 23, Table 1), TsOH (Entry 24, Table 1), and HCl (Entry 25, Table 1) are common acid catalysts known to characterize similar sugar polymerization products (29–32%), they did not offer the synergistic advantages of IL@SGO. This superiority is due to the integrated functions of SGO (enhanced stability and surface area) and IL (enhanced reaction selectivity). The design of hybrid catalysts such as IL@SGO is a good strategy for improving the reaction efficiency. The volume of the solvent is one of the most significant factors that affects the yield of the main product. In particular, the yield increased significantly going from 2 to 4 mL of toluene (Entries 35 and 37, Table 1), ultimately affording a 41% yield. However, by increasing the volume to 6 mL, a slight decrease was observed (38%, Entry 38, Table 1). This means that overly dilute conditions suppress the reactant-catalyst collisions. Solvent volumes should be optimized to maintain most of the kinetic benefits of mixing and progress but avoid excessive dilution. Control experiments in the absence of a solvent (Entry 28, Table 1) or a catalyst (Entry 27, Table 1) yielded negligible results (5% and 14%, respectively). This highlights the importance of having both elements for the reaction to occur properly. These controls confirmed the pivotal role of IL@SGO and toluene in mediating the reaction mechanism. Additionally, the reactions between each pair of substrates were also carried out under the same optimal condition and checked by TLC for comparison of the main product 2,3-diphenyl-4-thiazolidinone to explain the incomplete conversion of the reaction. The yield of the reactions can be affected by some side products, which are formed through the reaction of each pair.[42,43] The side reactions are mentioned in the ESI Scheme S2 and Section S2.†

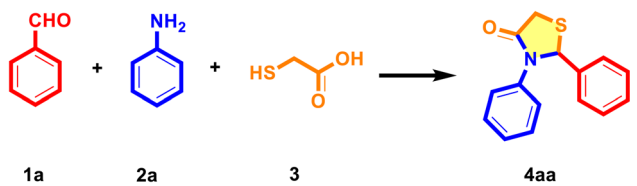

Scheme 2 Synthesis of 2,3-diphenyl-4-thiazolidinone (**4aa**).

Table 1 Optimization of reaction conditions[a]

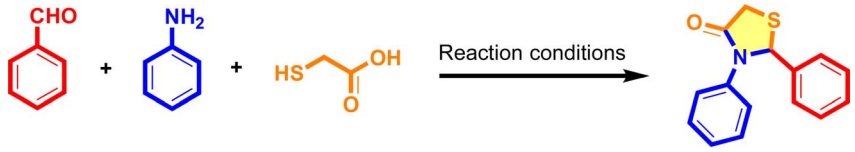

1a 2a 3 4aa

Entry	Temp. (°C)	Time (h)	Solvents	Volume of solvent (mL)	Catalysts	Loading of catalyst (mg)	Isolated yield[b] (%)
1	RT	8	Toluene	5	IL@SGO	5	16
2	60						21
3	80						32
4	100						30
5	120						29
6	80	5	Toluene	5	IL@SGO	5	27
7		6					28
8		7					28
9		9					37
10		10					36
11	80	9	Ethanol	5	IL@SGO	5	3(5)[c]
12			THF				13
13			H_2O				1(1)[c]
14			Ethyl acetate				24
15			Acetonitrile				1(1)[c]
16			DMF				2(7)[c]
17			Cyclohexane				2(1)[c]
18			*n*-Hexane				5(9)[c]
19			None	0			7(5)[c]
20	80	9	Toluene	5	GO	5	25
21					SGO		32
22					IL		31
23					H_2SO_4		29
24					TsOH		30
25					HCl		32
26					H_3PO_4		22
27					None	0	14
28	80	9	None	0	None	0	5(5)[c]
29			Toluene	5	IL@SGO	1	30
30						3	34
31						5	37
32						7	42
33						10	41
34	80	9	None	0	IL@SGO	7	15
35			Toluene	2			22
36				3			40
37				4			41
38				6			38

[a] Reaction conditions: benzaldehyde (1 mmol), aniline (1 mmol), and mercaptoacetic acid (1 mmol). [b] Isolated yield by crystallization in ethanol (5 mL). [c] The reactions were conducted by microwave.

The reaction conditions investigated were used to investigate the efficiency and utility of the synthesis procedure based on several substrates. The aim of this study was to evaluate the efficiency and versatility of the method in the synthesis of various 4-thiazolidinone derivatives using IL@SGO as the catalyst. The synthesis of 4-thiazolidinone derivatives was carried out between aldehydes (1.0 mmol), anilines (1.0 mmol), and mercaptoacetic acid (1 mmol) in the presence of toluene (5 mL) and IL@SGO (7 mg) at 80 °C for 9 h, and the results were recorded as acceptable to good (Scheme 3). These substituents, in a broad sense, can be classified as electron-donating groups (EDGs) and electron-withdrawing groups (EWGs), both of which significantly alter the electronic and steric environments of the reactions. EWGs include groups such as halogens (–F, –Cl, and –Br) and nitro ($-NO_2$) that remove electron density from the aromatic ring, mainly *via* inductive effects. Under certain conditions, these groups can stabilize transition states or intermediates through delocalization of negative charges,

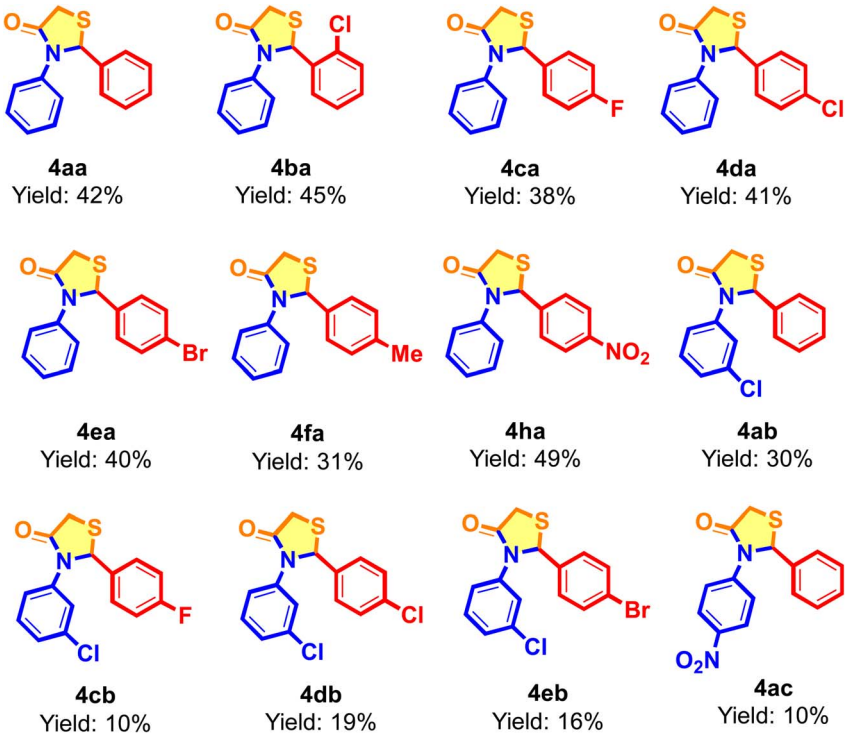

Scheme 3 Scope of 4-thiazolidinones. Reaction conditions: benzaldehyde derivatives (1 mmol), aniline derivatives (1 mmol), mercaptoacetic acid (1 mmol), IL@SGO (7 mg), toluene (5 mL), 80 °C, 9 hours. Isolated yield by crystallization in ethanol (5 mL).

thereby enhancing the reactivity. However, if one introduces a strong deactivating group, then one can do oxidization of the ring, and the reaction will cease as with the example above. Electron-withdrawing groups (EWGs) such as $-NO_2$ withdraw the electron density from the aromatic system through inductive or resonance effects. Groups that donate electrons to the aromatic system increase the nucleophilicity of the ring and promote reactivity. However, steric hindrance caused by these groups, especially at the *ortho* position, can hinder accessibility to reactive sites, thereby cutting yields. This duality often results in varied and position-dependent impacts on yields. Halogens are widely known for their moderate electron-withdrawing properties and relatively small steric footprints. As can be seen from Scheme 3, halogen-substituted compounds (**4ca**, **4da**, and **4ea**) displayed yields ranging from 38% to 41%. These results illustrated the trade-off between electronic stabilization and steric hindrance (38% yield of compound **4ca**). This small size of fluorine reduces steric hindrance, but some strong electronegativity of intermediates, making the reactivity lower than that of other larger sizes such as chlorine and bromine. The yield obtained with compound **4da** was 41%, slightly better than what was obtained with fluorine. Chlorine's larger size and weaker electronegativity than fluorine give a better balance between steric and electronic effects. For example, the proposed compound, **4ea**, gave a yield of 40% like chlorine. Bromine has an even larger atomic radius and more steric bulk and also greater polarizability, which may stabilize transition states. Nitro ($-NO_2$) groups are among the most potent electron-withdrawing substituents due to their capacity to delocalize negative charge *via* resonance and inductive effects. The moderate reactivity of **4fa** (31% yield) was due to the *para*-positioned nitro group, which reduced steric hindrance. However, the yield was lower than that of halogenated derivatives because of the strong electron-withdrawing effect. The *ortho*-positioned nitro group in **4ac** (10% yield) caused a lot of steric hindrance, and the fact that it pulled electrons away from the molecule makes the yield much lower. The methyl (–Me) group was a weak electron-donating group, contributing electron density *via* its inductive effect. It turned out that the *para*-positioned methyl group had the highest yield (49%), which means that its electron-donating properties made it more reactive without creating any steric problems. Positional differences (*e.g.*, *ortho*) may diminish yields due to steric obstruction. The methoxy (–OMe) group was a potent electron-donating group, providing electron density *via* resonance while exerting inductive withdrawal. The reaction was almost non-existent for methoxy-substituted compounds indicate that steric hindrance at the *ortho* position or excessive electron donation may interfere with the reaction process. Positional isomerism (*ortho*, *meta* or *para*) plays an important role in influencing the yield of products through the stereochemical and electron-donating effects of the reaction sites. When substituents are in the *ortho* position of compounds, they often face a lot of stereochemical hindrance, which makes them less reactive. This is why the product yields were low at *ortho*-NO_2 and *ortho*-OCH_3 positions. When aldehydes were used to synthesize compounds with substituents at the *para* position on the arene ring, there was less steric hindrance, which means

that more of the product was formed. However, the electronic effect was stronger, which achieved a high yield of about 49% with **4ha**. When anilines were added to products, the substituents were put in the *ortho*, *meta*, and *para* positions behind the amino group. This is because of the electronic effects and a strong steric hindrance effect, which made the amino group much less reactive.

2.3. Proposed reaction mechanism for the synthesis of 4aa

The reaction mechanism depicted involves a solid-supported organocatalyst (SGO) functionalized with quaternary ammonium groups and other active sites, facilitating multi-step transformation (Scheme 4). The objective of this proposed reaction process was to demonstrate how IL@SGO functions as a catalyst, interacting with the reactants to produce the desired product. In the initial phase, the surface of IL@SGO was endowed with quaternary ammonium salt functional groups that stabilize reaction intermediates and enhance catalytic efficiency. Upon activation of the carbonyl (–C=O) group in benzaldehyde, a nucleophilic addition of an amino group (–NH_2) from the aniline substrate occurred, resulting in the formation of an imine(I) intermediate *via* a typical addition–elimination mechanism. The amino group nucleophilically attacked electrophilic carbonyl carbon, resulting in the release of water. Upon interaction with the imine(I) intermediate, water decomposes, liberating the amine component and regenerating the carbonyl group. This hydrolysis step was essential for modifying the surface functionality of IL@SGO, enabling the catalyst to participate in subsequent reaction cycles. The thiol group (–SH) reacted with the intermediate(I) following hydrolysis under IL@SGO conditions. By means of interactions with the functional groups on the surface of IL@SGO, the nucleophilic assault produces a thioester intermediate(II). The ultimate result of intermediate(II) was intramolecular cyclization. The catalyst stayed whole throughout the procedure and is rebuilt at the end of the reaction; regeneration guarantees IL@SGO's reusability for several cycles, therefore stressing the environmental and financial advantages of catalyst use.

2.4. Reusability of the IL@SGO catalyst in the synthesis of 4aa

Two key elements significantly influence the efficiency of the green chemistry method in the newly developed protocol: the stability and recyclability of the IL@SGO catalyst. The catalyst was filtered from the reaction mixture and recycled after washing with acetone. This process was tested with several substrates including benzaldehyde (1 mmol), aniline (1 mmol), and mercaptoacetic acid (1 mmol), demonstrating repeated use without any significant loss of activity. However, over multiple runs (0 to 4), the yield of **4aa** showed a gradual decline, indicating slow deactivation of the IL@SGO catalyst. The leaching of functionalized IL moieties might diminish active site availability, while the accumulation of by-products could block these sites, and repeated reactions could harm the SGO's structural integrity. Despite this decline, the catalyst maintained reasonable activity, achieving a yield of 27% in run 4 after four cycles.

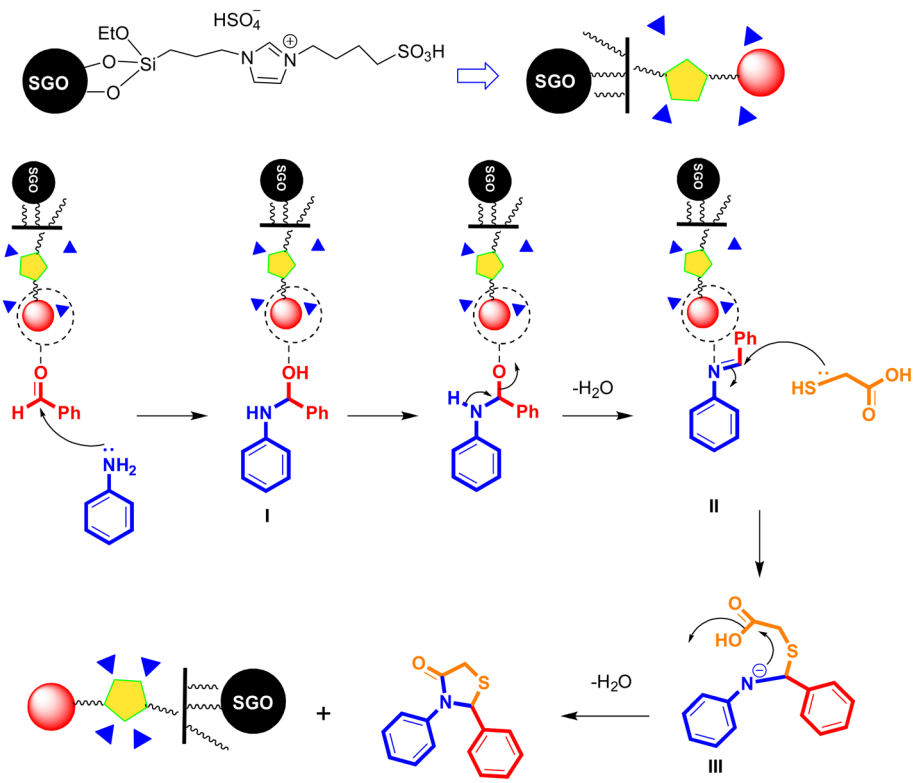

Scheme 4 Proposed reaction mechanism for the synthesis of **4aa**.

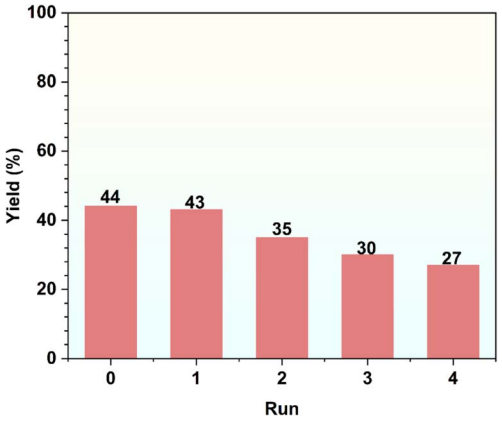

Fig. 9 Reusability of IL@SGO through catalysis in the synthesis process of **4aa**.

This suggested that IL@SGO can be reused, and enhancements in reaction conditions or regeneration methods could improve its recyclability. Washing or activating the catalyst between cycles maintained over 60% of its initial activity after four cycles (Fig. 9).

Fig. S1† presents the FT-IR spectra comparing IL@SGO and its recovery process. In the IL@SGO recovery spectrum, the decline in O–H band at 3200–3600 cm^{-1} suggested a partial loss of hydroxyl groups. Furthermore, the decline in the intensity of aliphatic and aromatic C–H stretching vibrations indicated that the IL may have experienced partial removal or decomposition. A more intense peak in the IL@SGO spectrum suggested stronger IL-GO interactions, while shifts and reduced intensity in the recovery spectrum imply structural changes like esterification or chemical degradation. The peaks associated with C=C and C=N stretching (1500–1600 cm^{-1}) were assigned to the aromatic rings and imine groups, with the decline in these peaks hinting at disrupted IL-GO π–π stacking interactions. Additionally, a notable drop in S=O band's strength in the recovery spectrum suggested sulfur group separation, implying instability of the IL under these conditions. The fingerprint area (500–1500 cm^{-1}) showed notable differences between the two spectra, with the IL@SGO spectrum displaying more complex vibrations than the less intense IL@SGO recovery spectrum, indicating a loss of functional variety and structural breakdown of the IL-GO composite during recovery. The shifts and intensity reductions in characteristic peaks (–OH, C=O, C–H, S=O) suggested that the recovery process adversely affects IL-GO interactions, leading to structural changes and loss of functional groups, particularly oxygen-containing ones.

Fig. S2† shows the TGA (Thermogravimetric Analysis) curves for IL@SGO (red line) and IL@SGO recovery (blue line). Both materials experience a minor weight loss below ~150 °C due to evaporated moisture, indicating similar surface moisture levels. However, IL@SGO recovery showed faster weight loss, particularly beyond 300 °C, suggesting reduced thermal stability from structural changes during recovery. Above ~500 °C, the weight loss indicated breakdown of stable elements such as sulfur and carbon. IL@SGO maintains a higher residual weight, indicating greater stability and possibly higher carbon content than the recovered material. This illustrated how recovery affected thermal stability: IL@SGO demonstrated greater resistance and slower decomposition, while recovery may compromise structural integrity and thermal behavior. Both materials remained stable up to ~300 °C, making them suitable for low-temperature applications.

Fig. S3† presents the SEM (Scanning Electron Microscopy) images and corresponding particle size distribution histograms for IL@SGO (top row) and IL@SGO recovery (bottom row). In contrast, the SEM image of recovered IL@SGO showed a less porous, more aggregated structure with smoother surfaces and less distinct particles, indicating partial collapse of the porous framework during recovery. The original IL@SGO catalyst had a peak particle size distribution in the 40–60 μm range, indicating homogeneity, while the recovered IL@SGO peaks at 60–80 μm reflect a broader size distribution due to particle agglomeration, likely from thermal or mechanical factors. This process decreased porosity and increased aggregation, potentially compromising the material's catalytic performance, as larger particles from the IL@SGO recovery may reduce the dispersion efficiency.

EDX spectroscopy revealed changes in the chemical composition of IL@SGO before and after recovery (Fig. S4†). After recovery, the C content decreased from 62.66 to 42.35%, suggesting loss or degradation of organic materials, while the O content increased, indicating possible oxidation or rearrangement. Notably, the S content dramatically increased from 4.33% to 25.42%, suggesting the adsorption of sulfur-rich species during recovery. The Si concentration dropped slightly to 1.02%, potentially indicating the partial dissociation of the GO structure, while the Cl levels remained unchanged. Overall, the recovery process led to a significant decrease in carbon content and a marked increase in sulfur content.

The microscopic images of IL@SGO before and after recovery revealed notable structural changes; IL@SGO seems to be quite porous with unequal particle distribution, which qualified for adsorption or catalysis uses (Fig. S5†). After recovery, the intensity and homogeneity of C and O decreased, aligning with organic material loss, while S became strong and localized, indicating its build-up. Cl remained less prominent but showed some intensity change, and Si followed a similar trend, suggesting decreased GO separation. Post-recovery, sulfur prominently formed localized areas, while carbon distribution diminished, confirming partial rearrangement of the IL and GO structures along with sulfur adsorption.

2.5. Leaching test

In the context of synthesis, particularly in materials science, chemistry, or environmental science, a leaching test is used to assess the potential for leaching of certain substances. In this experiment, a leaching test was applied to evaluate the sulfur content existing in the reaction before and after removing the catalyst out of the reaction. The leaching test experiment was conducted to characterize the chemical and physical properties of the materials, which suggest the effect of the material on

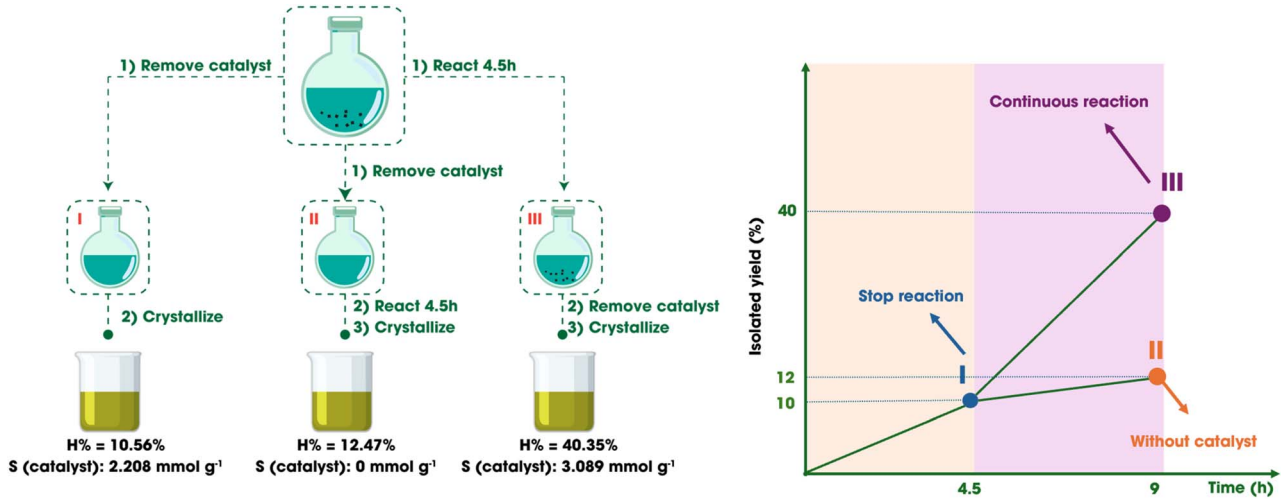

Fig. 10 Procedure for leaching tests: (I) reaction stopped; (II) reaction without IL@SGO; and (III) continuous reaction with IL@SGO.

nature in real applications. In this study, the mixture of benzaldehyde (3 mmol, 318 mg), aniline (3 mmol, 279 mg), mercaptoacetic acid (3 mmol, 276 mg), IL@SGO (21 mg), and toluene (15.0 mL) was heated at 80 °C. After 4.5 hours of reactions, the solution containing the solid catalyst was divided into 3 sections (Fig. 10). The ICP-OES method was used to measure the content of sulfur remaining in the catalyst of each reaction part.

In section (I), IL@SGO was separated from the reaction mixture, and the product solution was subjected to crystallization in 5 mL of ethanol. Subsequently, the main product was obtained with a yield of approximately 10%, and the sulfur content retained in the catalyst was determined to be 2.208 mmol g^{-1}.

In section (II), IL@SGO was separated from the reaction mixture, and the reaction proceeded with continuous stirring for the remaining 4.5 hours. Upon completion, the reaction mixture was crystallized in 5 mL of ethanol, yielding approximately 12% of the main product. At this stage, ICP-OES analysis confirmed the absence of sulfur leaching from the catalyst into the solution.

In section (III), the reaction mixture was allowed to continue for the remaining 4.5 hours. After the reaction was completed, IL@SGO was removed, and crystallization of the reaction mixture was carried out in 5 mL of ethanol. For the remaining reaction under optimal conditions, the yield of the main product was about 40% and the content of sulfur which remained in the catalyst was determined to be about 3.089 mmol g^{-1}.

2.6. Large-scale synthesis of 4aa

Scheme 5 presents reaction demonstrations, showing a three-component synthesis producing chemical **4aa**. Benzaldehyde (**1a**), aniline (**2a**), and mercaptoacetic acid (**3**) were used as starting materials in equimolar amounts of 5 mmol each. IL@SGO (35 mg) was present during the process acting as a catalyst. The reaction was carried out at 80 °C for 9 h with toluene (25 mL) as the solvent. The yield of product **4aa** was 44%. The product **4aa**'s structure suggests that, most likely by a sequence of condensation, cyclization, and substitution, the reaction generates a sulfur-containing heterocyclic ring. IL@SGO helps the condensation and cyclization processes, improving the general reaction efficiency.

2.7. Assessment of green metrics

Recently, the development of sustainable and environmentally friendly methods to produce organic compounds has received much attention. The use of IL@SGO as a catalyst for synthesizing 4-thiazolidinone frameworks was highlighted in this field. This method has been shown to have big benefits for the environment and efficiency. This approach was characterized by several favorable environmental metrics. The low Environmental-factor (E-factor) of 1.28 means that almost no waste was produced during the reaction, which makes it a more environmentally friendly choice than traditional methods of synthesis. Furthermore, the high atom economy (AE) of 89.28% indicated that most of the reactant atoms were included in the intended product, therefore lowering the resource usage. However, the actual atom efficiency (AEf) was lower at 43.75%,

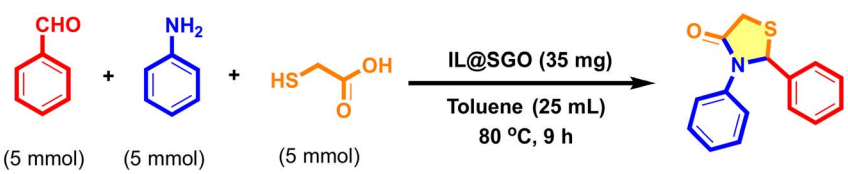

Scheme 5 Investigation of the scale-up process in **4aa** production using the IL@SGO catalyst.

which represented some atoms that were not successfully used in the process of creating the final product. Furthermore, the process mass intensity (PMI) was relatively low at 2.32, signifying an efficient use of raw materials. The carbon efficiency (CE) of 49%, however, means that almost half of the carbon atoms are not efficiently added to the target compound. This means that the process could be improved even more. The reaction mass efficiency (RME) was 43.74%, reflecting a modest ratio between the mass of the produced product and the total mass of the reactants consumed. Considering all these elements, this approach highlighted its potential as a greener substitute in organic synthesis by obtaining a reasonable eco-score of 57.5%. IL@SGO as a catalyst improved the sustainability of 4-thiazolidinone synthesis and reduced environmental impacts. The balance between high efficiency and environmental friendliness demonstrated its significance in promoting sustainable chemistry. This advancement opens the path for creative, low-impact synthetic techniques in the future and marks a vital first step toward greener solutions.[44–47] (The calculation data are given in the ESI†)

2.8. Comparative analysis of the present method and alternative strategies for 4aa synthesis

Table 2 compares different reaction conditions for the synthesis of **4aa** and their respective yields. By using NMPs@SiO_2-IL in water under reflux for 1 hour, a yield of 48% was achieved. By employing Baker's yeast in THF at room temperature for 40 hours, the reaction showed the highest yield of 60%, though with a significantly prolonged reaction time. H_2SO_4–SiO_2 in toluene at 100 °C achieved 55% yield in 5 hours. In this study, IL@SGO (7 mg) was added to toluene and reacted at 80 °C for 9 hours, yielding 42%. However, this approach might offer benefits in terms of environmental sustainability or catalyst recyclability. Table 2 illustrates that although all the previously suggested catalysts are appropriate for the designated synthesis conditions, most exhibit certain drawbacks. The drawbacks included elevated temperatures, extended reaction durations, excessive catalyst usage, reliance on hazardous catalysts or toxic organic solvents, and complex work-up procedures.

3. Experimental

3.1. Chemical

The leaves of *Syzygium nervosum* applied in the experiments were purchased from Cu Chi District, Ho Chi Minh City, Vietnam. 2-Chlorobenzaldehyde (99%) was purchased from ACROS Organic (India) and 4-chloroaniline (99%) from Sigma Aldrich (USA). 4-Fluorobenzaldehyde (98.49%) was supplied by Bidepharm (China) and 4-methylbenzaldehyde (97%) by Merck. 4-Nitrobenzaldehyde (98.0%) was supplied by Thermo Scientific (USA). Common solvents including acetone (95%), acetonitrile (>99%), ethanol (99%), diethyl ether (≥99.5%) and dimethylformamide (≥99.5%) were obtained from Chemsol, Vietnam. Acids used in the research including Hydrochloric acid (36.0–38.0%) and phosphoric acid (85%) were purchased from Xilong (China) and GHTECH (JHD), respectively. *p*-Toluenesulfonic acid (99%) was obtained from Sigma Aldrich (USA) and sulfanilic acid (90%) was obtained from Scharlau (Spain). Additionally, mercaptoacetic acid (90%) was obtained from Shanghai Zhanyun (China). Sodium hydroxide (>96%), sodium nitrate (99%), and sodium nitrite (99%) were all sourced from Xilong.

3.2. Techniques for analysis

^{1}H-NMR and ^{13}C-NMR spectra were recorded using a Bruker Avance 500 MHz spectrometer, with DMSO-d_6 as the solvent and reference standard. The melting points of the samples were measured using a Buchi B-545 apparatus. The FT-IR spectrum was recorded using a Bruker E400 FT-IR spectrometer. Thermogravimetric analysis (TGA) was performed using a Q-500 device, by heating the samples at a rate of 5 °C per minute under a controlled air flow. P-XRD data were acquired using a Bruker D8 Advance diffractometer equipped with a Ni-filtered Cu Kα radiation source (λ = 1.54059 Å). The material's morphology and structure were examined by scanning electron microscopy (SEM) using a Hitachi S-4800, coupled with an XZS-107T digital microscope and an NHV-CAM camera, and processed using the eScope software. Nitrogen adsorption–desorption isotherms were recorded at 77 K using a Quantachrome NOVA 3200e system. Energy-dispersive X-ray spectroscopy (EDX) was performed using an EMAX energy EX-400 EDX instrument. Finally, high-resolution mass spectrometry (HRMS) was carried out using a Bruker micrOTOF-QII spectrometer in the positive electrospray ionization (ESI) mode, at an ionization energy of 80 eV.

3.3. Preparation of IL@SGO from *Syzygium nervosum* leaves

3.3.1. Preparation of GO. The initial material employed was the leaf residue of *Syzygium nervosum*, which was carbonized in an inert environment at 650 °C for 3 hours, leading to the production of graphite.[26] Then, GO was synthesized using modified Hummer's method.[27]

3.3.2. Preparation of SGO (sulfonated graphene oxide). The aryl diazonium solution for GO sulfonation was prepared as

Table 2 Comparison of our findings with previously published data on the synthesis of **4aa**

Entry	Condition reaction	Temp. (°C)	Time (h)	Yield (%)	Ref.
1	NMPs@SiO_2-IL (0.0007 g), H_2O	Reflux	1	48	48
2	Baker's yeast (2 g), THF	RT	40	60	49
3	H_2SO_4–SiO_2 (10 mol%), toluene	100	5	55	50
4	IL@SGO (7 mg), toluene (5 mL)	80	9	42	This work

follows:[28] first, 0.5 g of sulfanilic acid was dissolved in 50 mL of 2% NaOH solution at 40 °C, followed by the addition of 0.2 g of $NaNO_2$. Once fully dissolved, 100 mL of ice-cold water and 10 mL of HCl were added to the solution under continuous stirring. The temperature was maintained at 0 °C for 15 minutes to form a diazonium salt. Subsequently, this aryl diazonium salt solution was gradually added dropwise to 200 mL of an aqueous GO solution (2.5 mg mL^{-1}). The resulting mixture was vigorously stirred in an ice-water bath for 4 hours. The product was then recovered by centrifugation, washed several times with water, and dried in an oven at 100 °C.

3.3.3. Preparation of IL. First, 1.7 g imidazole with 4.6 mL CPTES (3-chloropropyltriethoxysilane) was added into a 100 mL round-bottom flask. Then 25 mL Toluene was added to the flask and refluxed at 110 °C for 12 hours. The mixture was then subjected to rotary evaporation to obtain the yellow product N3PI (*N*-(3-propyltriethoxysilane)imidazole). Next, 0.71 g (10.5 mmol) 1,4-butanesultone was added dropwise to a 50 mL beaker containing 1.36 g (10 mmol) N3PI. Then, 15 mL toluene was added to the beaker and stirred for 45 minutes. The mixture was stirred for an additional 8 hours, and the solvent was removed by rotary evaporation. The resulting mixture was placed into a 100 mL round-bottom flask. After that, 15 mL EtOH was added to the round-bottom flask and stirred for 45 minutes. Then, 0.27 mL (10 mmol) 95% H_2SO_4 was added dropwise to the mixture. The mixture was stirred at 50 °C for 8 hours. The mixture was then subjected to rotary evaporation to obtain a bright yellow dual-acid IL product.[29]

3.3.4. Preparation of IL@SGO. First, 1.0 g of IL was added to a 100 mL round-bottom flask with 30 mL of EtOH. Then 2.0 g of SGO was added to the flask and refluxed for 24 hours. The mixture after refluxing was filtered and washed with diethyl ether. The product was dried at 100 °C to obtain the catalyst.[29]

3.4. General procedure for the synthesis of 4-thiazolidinone derivatives

The mixture of benzaldehydes (1 mmol), anilines (1 mmol), mercaptoacetic acid (1 mmol), IL@SGO (7 mg), and toluene (5 mL) was stirred at 80 °C for 9 hours. The progress of the reaction was observed by thin-layer chromatography (TLC). After the completion of the reaction, the mixture was allowed to cool at room temperature. Then, the mixture was filtered to separate the catalyst from the reaction solution. The IL@SGO catalyst was washed with diethyl ether and dried. The reaction solution was rotary evaporated to recover the solvent. Then, 5 mL of EtOH was added to induce crystallization. To obtain a pure product, it was washed several times with cold EtOH. The structure of the products were determined using ^{1}H NMR and ^{13}C NMR spectra.

3.5. General procedure for the recycling of IL@SGO

Following the reaction, the solid catalyst was separated and washed with distilled toluene (5 × 5 mL) and diethyl ether (5 × 3 mL). The washing process was monitored by TLC. The catalyst was then dried at 100 °C for the next reaction. The catalyst was reused under the same reaction conditions with a mixture of benzaldehyde, aniline, and mercaptoacetic acid. The weight of substrates for the next recovery reaction was calculated based on the weight of the catalyst, which can be recovered from each cycle. Data were collected after 4 recycling iterations.

3.6. Scale-up test process

A mixture of benzaldehyde (5 mmol, 0.5305 g), aniline (5 mmol, 0.4655 g), mercaptoacetic acid (5 mmol, 0.4605 g), IL@SGO catalyst (35 mg), and 25 mL of toluene was added into a 100 mL round-bottom flask. The reaction mixture was stirred at 80 °C for 9 hours and monitored by TLC using a 4 : 1 (*n*-hexane : acetone, v/v) solvent system. After the reaction was complete, the mixture was allowed to cool to room temperature and filtered to separate the catalyst and the reaction mixture. The catalyst, after separation, was washed several times by centrifugation with toluene solvent (3 × 5 mL) to remove impurities. It was then washed with diethyl ether (3 × 5 mL) and dried at 100 °C to recover the catalyst. The reaction mixture was subjected to rotary evaporation to recover the toluene solvent. Then, approximately 5–10 mL of EtOH was added to the mixture for crystallization. The product was washed with cold EtOH to remove unwanted impurities.

4. Conclusion

In conclusion, the article presented a comprehensive study of the synthesis, characterization, and catalytic application of ionic liquid-functionalized sulfur-doped graphene oxide (IL@SGO), containing Brønsted acid sites. The study began with the preparation and structural analysis of IL@SGO, detailing its synthesis from *Syzygium nervosum* leaves, functionalization with sulfonic acid groups, and integration with an ionic liquid (IL). Various analytical techniques including FT-IR spectroscopy, XRD, TGA, SEM, and EDX confirmed the successful modification and functionalization of the material. The catalytic efficiency of IL@SGO was evaluated in the one-pot synthesis of 4-thiazolidinone derivatives. The optimized reaction conditions were investigated on a variety of substrates to evaluate the efficiency and versatility of the synthetic protocol for 4-thiazolidinone derivatives. The study demonstrated excellent catalytic performance, achieving yields ranging from satisfactory to outstanding, highlighting the broad substrate compatibility of the method. The reusability studies indicated that IL@SGO maintains catalytic activity over multiple cycles. We anticipated that the produced 4-thiazolidinone compounds will have extensive applications in pharmaceutical and medicinal chemistry through the exploration of their pharmacological potential.

The study also assessed the environmental sustainability of the process using green chemistry metrics. IL@SGO-based catalysis exhibited high atom economy (89.28%) and a low environmental factor (E-factor = 1.28), supporting its potential as an eco-friendly alternative to organic synthesis. However, moderate carbon efficiency (49%) and reaction mass efficiency (43.74%) indicated room for further optimization. IL@SGO proves to be an effective, reusable, and environmentally

sustainable catalyst for the synthesis of 4-thiazolidinones, contributing to the advancement of green chemistry. Future research may be focused on improving its stability and optimizing the reaction conditions to enhance the efficiency and sustainability.

Data availability

The authors confirm that the data supporting the findings of this study are available within the article. Raw data that support the findings of this study are available from the corresponding author upon reasonable request.

Author contributions

Quang Nhat Trinh: investigation, methodology, resources, formal analysis, validation, data curation, and writing – original draft. Linh Dieu Nguyen: formal analysis, data curation, and writing – original draft. Hai Truong Nguyen: methodology, resources, formal analysis, validation, data curation, writing – review and editing, and supervision.

Conflicts of interest

The authors declare that they have no known competing financial interests or personal relationships that could have appeared to influence the work reported in this paper.

References

1 R. Cai, X. Pei, H. Pan, K. Wan, H. Chen, Z. Zhang and Y. Zhang, *Energy Fuels*, 2020, **34**, 11771–11790.
2 S. Ao, B. Changmai, C. Vanlalveni, M. V. L. Chhandama, A. E. H. Wheatley and S. L. Rokhum, *Renewable Energy*, 2024, **223**, 120031.
3 A. B. Seabra, A. J. Paula, R. de Lima, O. L. Alves and N. Durán, *Chem. Res. Toxicol.*, 2014, **27**, 159–168.
4 A. Ghulam, O. Leitão dos Santos, L. Hazeem, B. Backx, M. Bououdina and S. Bellucci, *J. Funct. Biomater.*, 2022, **13**, 77.
5 N. I. Kovtyukhova, P. J. Ollivier, B. R. Martin, T. E. Mallouk, S. A. Chizhik, E. V. Buzaneva and A. D. Gorchinskiy, *Chem. Mater.*, 1999, **11**, 771–778.
6 K. Spyrou and P. Rudolf, in *Functionalization of Graphene*, 2014, pp. 1–20, DOI: 10.1002/9783527672790.ch1.
7 F. G. Torres, O. P. Troncoso, L. Rodriguez and G. E. De-la-Torre, *Sustainable Mater. Technol.*, 2021, **29**, e00310.
8 F. Wang, Y. Zhang, B. B. Zhang, R. Y. Hong, M. R. Kumar and C. R. Xie, *Composites, Part B*, 2015, **83**, 66–74.
9 X. Jing, Z. Li, B. Lu, Y. Han, Y. Chi and C. Hu, *Appl. Catal., A*, 2020, **598**, 117613.
10 X. Kong, P. Nie, L. Shi, M. Hu, P. Zhang, X. Li, Z. Wang and X. Liu, *Chem. Eng. J.*, 2021, **425**, 131598.
11 H. Zhang, Q. Zhang, L. Zhang, T. Pei, L. Dong, P. Zhou, C. Li and L. Xia, *Chem. Eng. J.*, 2018, **334**, 285–295.
12 R. Gusain, N. Kumar, S. Seyedin and Y. Jiang, *Adv. Sustainable Syst.*, 2024, **8**, 2400341.
13 S. Rubesh Ashok Kumar, D. Vasvini Mary, G. A. Suganya Josephine and M. A. Riswan Ahamed, *Hybrid Adv.*, 2024, **5**, 100168.
14 G. Küçükgüzel, A. Kocatepe, E. De Clercq, F. Şahin and M. Güllüce, *Eur. J. Med. Chem.*, 2006, **41**, 353–359.
15 E. Pitta, E. Tsolaki, A. Geronikaki, J. Petrović, J. Glamočlija, M. Soković, E. Crespan, G. Maga, S. S. Bhunia and A. K. Saxena, *MedChemComm*, 2015, **6**, 319–326.
16 P. Roszczenko, S. Holota, O. K. Szewczyk, R. Dudchak, K. Bielawski, A. Bielawska and R. Lesyk, *Int. J. Mol. Sci.*, 2022, **23**, 13135.
17 A. Gornowicz, R. Lesyk, R. Czarnomysy, S. Holota, Y. Shepeta, B. Popławska, M. Podolak, W. Szymanowski, K. Bielawski and A. Bielawska, *Int. J. Mol. Sci.*, 2023, **24**, 6791.
18 M. Mishchenko, S. Shtrygol, D. Kaminskyy and R. Lesyk, *Sci. Pharm.*, 2020, **88**, 16.
19 A. Gupta, R. Singh, P. K. Sonar and S. K. Saraf, *Biochem. Res. Int.*, 2016, **2016**, 8086762.
20 V. N. Koshelev, O. V. Primerova, S. V. Vorobyev, A. S. Stupnikova and L. V. Ivanova, *Appl. Sci.*, 2023, **13**, 13112.
21 S. Nirwan, V. Chahal and R. Kakkar, *J. Heterocycl. Chem.*, 2019, **56**, 1239–1253.
22 L. P. Zorba, I. Stylianakis, N. Tsoureas, A. Kolocouris and G. C. Vougioukalakis, *J. Org. Chem.*, 2024, **89**, 7727–7740.
23 S. Sepehri, G. Farhadi, M. Maghbul, F. Nasiri, M. A. Faramarzi, K. Mahnam, S. Mojtabavi, M. Mahdavi and Z. Moharrami Oranj, *Heliyon*, 2024, **10**, e36408.
24 A. A. Hassan, N. K. Mohamed, K. M. A. El-Shaieb, H. N. Tawfeek, S. Bräse and M. Nieger, *Arab. J. Chem.*, 2019, **12**, 289–294.
25 A. Sharma, D. Sharma, N. Saini, S. V. Sharma, V. K. Thakur, R. K. Goyal and P. C. Sharma, *Cancer Metastasis Rev.*, 2023, **42**, 847–889.
26 A. Faiz, C. Azurahanim, Y. Yaakob, A. Suriani and M. Ain, *Mater. Res. Express*, 2020, **7**, 015613.
27 R. Ramli and R. Hidayat, *Graphene Oxide Based on Biomass Waste: Synthesis and Applications*, Intech Open, 2023.
28 M. T. Rezaei, S. Valizadeh and L. Naji, *Thin Solid Films*, 2021, **728**, 138688.
29 Q. Zhang, J. Luo and Y. Wei, *Green Chem.*, 2010, **12**, 2246–2254.
30 S. Verma, S. Verma, A. Agrwal and V. Kasana, *Polycycl. Aromat. Comp.*, 2024, **44**, 2442–2457.
31 N. Karikalan, R. Karthik, S.-M. Chen, C. Karuppiah and A. Elangovan, *Sci. Rep.*, 2017, **7**, 2494.
32 W. Fam, J. Mansouri, H. Li, J. Hou and V. Chen, *ACS Appl. Mater. Interfaces*, 2018, **10**, 7389–7400.
33 B. Manna and C. R. Raj, *ACS Sustainable Chem. Eng.*, 2018, **6**, 6175–6182.
34 J. Guo, W. Wang, Y. Li, J. Liang, Q. Zhu, J. Li and X. Wang, *RSC Adv.*, 2020, **10**, 26460–26466.
35 Y.-X. Ma, W.-J. Shao, W. Sun, Y.-L. Kou, X. Li and H.-P. Yang, *Appl. Surf. Sci.*, 2018, **459**, 544–553.
36 R. Sedghi, B. Heidari and M. Yassari, *J. Colloid Interface Sci.*, 2017, **503**, 47–56.
37 Z. Yang, Z. Yao, G. Li, G. Fang, H. Nie, Z. Liu, X. Zhou, X. A. Chen and S. Huang, *ACS Nano*, 2012, **6**, 205–211.

38 J. Wang, R. Ma, Z. Zhou, G. Liu and Q. Liu, *Sci. Rep.*, 2015, **5**, 9304.
39 A. S. Siddiqui, A. Hayat, M. H. Nawaz, M. A. Ahmad and M. Nasir, *Appl. Surf. Sci.*, 2020, **509**, 144695.
40 V. Sayyab, Z. Hussain, A. Noor, H. Qayyum and H. Shafique, *J. Bionanosci.*, 2025, **15**, 1–13.
41 S. Zhang, H. Wang, J. Liu and C. Bao, *Mater. Lett.*, 2020, **261**, 127098.
42 J. Luo, Z. Zhong, H. Ji, J. Chen, J. Zhao and F. Zhang, *J. Sulphur Chem.*, 2016, **37**, 438–449.
43 R. Verma, N. P. Lamba, A. Dandia, A. Srivastava, K. Modi, M. S. Chauhan and J. Prasad, *Sci. Rep.*, 2022, **12**, 9636.
44 R. A. Sheldon, *ACS Sustainable Chem. Eng.*, 2018, **6**, 32–48.
45 D. J. C. Constable, A. D. Curzons and V. L. Cunningham, *Green Chem.*, 2002, **4**, 521–527.
46 K. Van Aken, L. Strekowski and L. Patiny, *Beilstein J. Org. Chem.*, 2006, **2**, 3.
47 N. Sahiba, A. Sethiya, J. Soni and S. Agarwal, *ChemistrySelect*, 2020, **5**, 13076–13080.
48 N. Azgomi and M. Mokhtary, *J. Mol. Catal. A: Chem.*, 2015, **398**, 58–64.
49 U. R. Pratap, D. V. Jawale, M. R. Bhosle and R. A. Mane, *Tetrahedron Lett.*, 2011, **52**, 1689–1691.
50 D. Kumar, M. Sonawane, B. Pujala, V. K. Jain, S. Bhagat and A. K. Chakraborti, *Green Chem.*, 2013, **15**, 2872–2884.